

Long-Range Rendezvous and Docking Maneuver Control of Satellite using Cross-Feedback Sliding Mode Controller

Vedant Vivek Kini[†]

*Department of Aerospace Engineering
Indian Institute of Technology Kharagpur
West Bengal, 721302, India
vedantkini21@kgpian.iitkgp.ac.in*

Dantu Phani Surya[†]

*Department of Aerospace Engineering
Indian Institute of Technology Kharagpur
West Bengal, 721302, India
suryadantu18@kgpian.iitkgp.ac.in*

Rakesh Kumar Sahoo^{*}

*Department of Aerospace Engineering
Indian Institute of Technology Kharagpur
West Bengal, 721302, India
rakesh.sahoo266@gmail.com*

Manoranjan Sinha

*Department of Aerospace Engineering
Indian Institute of Technology Kharagpur
West Bengal, 721302, India
masinha@aero.iitkgp.ac.in*

Abstract—Satellite rendezvous and docking (RvD) maneuvers are essential for satellite servicing and in-orbit assembly. Traditional approaches often treat translational and rotational motions independently, simplifying control design but potentially leading to inefficiencies in maneuver time and fuel consumption. To address these challenges, a novel cross-feedback sliding mode controller has been proposed, developing an interdependent regulation system for translational and rotational motion. This method decouples the relative translational and rotational motion of chaser satellite with respect to target satellite while incorporating cross-feedback mechanisms to account for their inherent coupling. By incorporating rotational state information into translational control laws and vice versa, the approach ensures coordinated adjustments, enhancing maneuver efficiency. The chaser satellite manages both translational and rotational adjustments to rendezvous and dock with the target satellite. The stability of the cross-feedback sliding mode controller is established within the Lyapunov framework, and simulation results substantiate the effectiveness of this strategy.

Index Terms—rendezvous, docking, cross-feedback control, sliding mode controller.

I. INTRODUCTION

Satellite rendezvous and docking (RvD) maneuvers are among the most intricate and mission-critical operations, requiring precise coordination between two satellite to achieve successful alignment and docking [1]. The rendezvous maneuver involves bringing the chaser satellite closer to the target [2], [3], [4]. This is followed by the docking phase, where precise alignment and a secure physical connection between their docking ports are achieved by rotating the chaser satellite or both satellites, depending on feasibility [5], [6]. These maneuvers are fundamental to a wide range of space

applications, including crewed spaceflight, orbital resupply missions, satellite servicing, and the in-orbit assembly of large space structures [7]. The significance of RvD is exemplified by missions such as ISRO's SpaDeX, which successfully demonstrated India's ability to autonomously dock two satellites in orbit. Such advancements underscore the critical role of precise guidance, navigation, and control strategies in ensuring mission success.

Traditionally, satellite RvD maneuvers have been designed by treating translational and rotational motion as independent processes [8]. Translational motion governs the satellite's trajectory in three-dimensional space, actuated using the thruster to regulate velocity and position. Conversely, rotational motion, or attitude dynamics, determines the satellite's orientation, actuated using reaction wheels and control moment gyroscope to generate the required torques. This decoupled approach simplifies the controller design and also reduces the computational requirement [9]. For instance, during the Apollo missions, the Lunar and Command Modules executed RvD maneuvers by sequentially adjusting position and orientation, reducing control complexity [10]. However, this stepwise approach resulted in increased maneuver duration and fuel consumption, as translational and rotational adjustments were performed separately. Given the stringent fuel constraints in space missions, such inefficiencies could impose operational limitations or even jeopardize mission success. Despite its conceptual simplicity, the independent treatment of translation and rotation overlooks the inherent coupling between these dynamics. In reality, satellite attitude changes influence trajectory by altering thrust direction and external force interactions. Neglecting these interdependencies can degrade maneuver accuracy, requiring additional corrections, increasing fuel consumption, and prolonging mission duration.

[†] Joint first authors

^{*} Corresponding author: rakesh.sahoo266@gmail.com

To address the limitations of the traditional decoupled approach and ensure robust and efficient RvD maneuvers, numerous studies in the literature have formulated translational and rotational dynamics within a unified control framework [11], [12] in close proximity of target satellite. Coupled motion control facilitates simultaneous adjustments in position and orientation, leading to improved maneuver efficiency by minimizing both time and fuel consumption. This integrated approach is particularly advantageous for close-proximity RvD operations [13], [14], [15]. However, the incorporation of coupled dynamics significantly increases the complexity of the mathematical model, making real-time implementation computationally intensive. Moreover, improper tuning of the control parameters may induce instability or unintended system behavior, as errors in one motion component can propagate and amplify, potentially compromising the overall maneuver performance.

In this paper, we have proposed a novel method for efficient long-range rendezvous and docking maneuvers to address the limitations of both decoupled and coupled approaches described above. This approach decouples the translational and rotational motion of each satellite, as in traditional decoupled methods, but introduces a cross-feedback sliding mode controller to account for the inherent coupling between these dynamics. Unlike conventional decoupled control, cross-feedback control establishes an interdependent regulation system by incorporating rotational state information into the translational control law and vice versa. This ensures that corrections in one domain (translational or rotational) are compensated by adjustments in the other, enabling a more coordinated and efficient maneuver. In this hybrid approach, the chaser satellite performs both translational and rotational motion, while the target satellite executes only rotational motion, optimizing the overall maneuver process.

The paper is organized as follows. In Section 2, the rigid body dynamics of both the chaser and target satellites are described, followed by the relative kinematics and dynamics of the chaser with respect to the target satellite. The trajectory constraints of fuel optimal rendezvous and docking maneuver is outlined in Section 3. Section 4 details the proposed cross-feedback sliding mode controller. Finally, Section 4 presents the simulation results, demonstrating the effectiveness of the proposed approach.

II. RIGID BODY DYNAMICS OF SATELLITES

This section presents the rigid body dynamic model of the target and the chaser satellite orbiting around the Earth. To model the dynamics three reference frames are defined as International Celestial Reference Frame (ICRF) [16] denoted by E_i , the chaser body-fixed frame denoted by E_c and the target body-fixed frame denoted by E_t .

A. Rigid Body Dynamics and Kinematics of Target Satellite

Let the position vector of the target satellite with respect to E_t be denoted by \tilde{p}_t , whereas the translational and angular velocity of target satellite w.r.t E_i frame be denoted by \tilde{v}_t

and $\tilde{\omega}_t$, respectively. The kinematics and dynamics of the translational motion of the target satellite can be described as

$$M_t \dot{\tilde{v}}_t + M_t \mathbf{\Omega}(\tilde{\omega}_t) \tilde{v}_t = \tilde{F}_{dt} + \tilde{F}_{j_2,t} \quad (1)$$

$$\dot{\tilde{p}}_t + \mathbf{\Omega}(\tilde{\omega}_t) \tilde{p}_t = \tilde{v}_t \quad (2)$$

where M_t is the mass of the target satellite, taken as 1000 kg, \tilde{F}_d and $\tilde{F}_{j_2,t}$ are the external disturbance force and J_2 perturbation force acting on the target satellite as shown in (3), respectively

$$\begin{aligned} F_{x_{j_2,t}} &= \frac{3}{2} \frac{\mu J_2 R_E^2}{|\tilde{p}_t|^5} \left[p_{tx} \left(5 \frac{p_{tx}^2}{|\tilde{p}_t|^2} \right) - 1 \right] \\ F_{y_{j_2,t}} &= \frac{3}{2} \frac{\mu J_2 R_E^2}{|\tilde{p}_t|^5} \left[p_{ty} \left(5 \frac{p_{ty}^2}{|\tilde{p}_t|^2} \right) - 1 \right] \\ F_{z_{j_2,t}} &= \frac{3}{2} \frac{\mu J_2 R_E^2}{|\tilde{p}_t|^5} \left[p_{tz} \left(5 \frac{p_{tz}^2}{|\tilde{p}_t|^2} \right) - 3 \right] \end{aligned} \quad (3)$$

where $J_2 = 0.00108263$ and $R_E = 6378$ km is the radius of earth. $\mathbf{\Omega}(\tilde{\omega}_t)$ represents the skew-symmetric matrix form of angular velocity vector $\tilde{\omega}_t$ defined as:

$$\mathbf{\Omega}(\tilde{\omega}_t) = \begin{bmatrix} 0 & -\omega_{tz} & \omega_{ty} \\ \omega_{tz} & 0 & -\omega_{tx} \\ -\omega_{ty} & \omega_{tx} & 0 \end{bmatrix}$$

The rotational kinematics and dynamics of the target satellite is described as given below.

$$\mathbf{J}_t \dot{\tilde{\omega}}_t = -\mathbf{\Omega}(\tilde{\omega}_t) \mathbf{J}_t \tilde{\omega}_t + \tilde{T}_{dt} + \tilde{T}_{gt} \quad (4)$$

where \tilde{T}_{dt} and \tilde{T}_{gt} represent the external disturbance torque and the gravity gradient torque acting on the target satellite as shown in (5); $\mathbf{J}_t \in \mathbb{R}^{3 \times 3}$ denotes the inertia matrix of the target satellite.

$$\begin{aligned} T_{gtx} &= \frac{3\mu}{2|\tilde{p}_t|^3} (J_z - J_y) \sin(2\phi_t) \cos^2(\theta_t) \\ T_{gty} &= \frac{3\mu}{2|\tilde{p}_t|^3} (J_z - J_x) \sin(2\theta_t) \cos^2(\phi_t) \\ T_{gtz} &= \frac{3\mu}{2|\tilde{p}_t|^3} (J_x - J_y) \sin(2\theta_t) \cos^2(\phi_t) \end{aligned} \quad (5)$$

where θ_t and ϕ_t are the pitch and roll angles of the target satellite. The attitude kinematics of the target satellite is given below:

$$\dot{\tilde{q}}_t = \mathbf{G}(\tilde{q}_t) \tilde{\omega}_t \quad (6)$$

where \tilde{q}_t is the Modified Rodrigues Parameters (MRPs) describing the attitude of the target satellite and $\mathbf{G}(\tilde{q}_t) \in \mathbb{R}^{4 \times 4}$ is defined as follows:

$$\mathbf{G}(\tilde{q}_t) = \frac{1}{4} (\mathbb{I}_3 (1 - \tilde{q}_t^T \tilde{q}_t) - 2\mathbf{\Omega}(\tilde{q}_t) + 2\tilde{q}_t \tilde{q}_t^T)$$

\mathbb{I}_3 represents the three dimensional identity matrix. The rotation matrix which transforms from target body-fixed frame to ICRF frame is given by

$$\mathbf{B}_t^i = \mathbb{I}_3 - \frac{4(1 - \tilde{q}_t^T \tilde{q}_t) \mathbf{\Omega}(\tilde{q}_t)}{(1 + \tilde{q}_t^T \tilde{q}_t)^2} + \frac{8\mathbf{\Omega}(\tilde{q}_t)^2}{(1 + \tilde{q}_t^T \tilde{q}_t)^2} \quad (7)$$

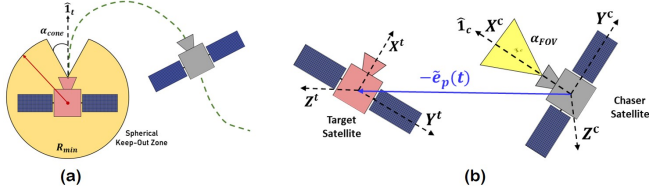


Fig. 1. Illustration of trajectory constraints for precise rendezvous and docking maneuver

B. Rigid Body Dynamics and Kinematics of Chaser Satellite

Let the position vector of the chaser satellite with respect to E_c be denoted by \tilde{p}_c , whereas the translational and angular velocity of chaser satellite w.r.t E_i frame be denoted by \tilde{v}_c and $\tilde{\omega}_c$, respectively. The kinematics and dynamics of the translational motion of the chaser satellite can be described as

$$M_c \dot{\tilde{v}}_c + M_c \mathbf{\Omega}(\tilde{\omega}_c) \tilde{v}_c = \tilde{F}_{dc} + \tilde{F}_{j_2,c} + \tilde{F}_c \quad (8)$$

$$\dot{\tilde{p}}_c + \mathbf{\Omega}(\tilde{\omega}_c) \tilde{p}_c = \tilde{v}_c \quad (9)$$

where M_c is the mass of the chaser satellite, \tilde{F}_{dc} , \tilde{F}_c and $\tilde{F}_{j_2,c}$ are the external disturbance force, control input force and J_2 perturbation force acting on the chaser satellite. The attitude dynamics and kinematics of the chaser satellite are given by:

$$\mathbf{J}_c \dot{\tilde{\omega}}_c = -\mathbf{\Omega}(\tilde{\omega}_c) \mathbf{J}_c \tilde{\omega}_c + \tilde{T}_{dc} + T_{gc} + \tilde{T}_c \quad (10)$$

where \mathbf{J}_c represents the inertia matrix of the chaser satellite, \tilde{T}_{dc} , \tilde{T}_c and \tilde{T}_{gc} are the external disturbance torque, control input torque and gravity-gradient torque acting on the chaser satellite and are of the same form as that of the target satellite as shown in (5). The attitude kinematics of the chaser satellite is given below:

$$\dot{\tilde{q}}_c = \mathbf{G}(\tilde{q}_c) \tilde{\omega}_c \quad (11)$$

where \tilde{q}_c is the Modified Rodrigues Parameters (MRPs) describing the attitude of the target satellite and $\mathbf{G}(\tilde{q}_c) \in \mathbb{R}^{4 \times 4}$ is of the same as that of target satellite (II-A). The rotation matrix which transforms from chaser body-fixed frame to ICRF frame is given by

$$\mathbf{B}_c^i = \mathbb{I}_3 - \frac{4(1 - \tilde{q}_c^c \tilde{q}_c) \mathbf{\Omega}(\tilde{q}_c)}{(1 + \tilde{q}_c^T \tilde{q}_c)^2} + \frac{8\mathbf{\Omega}(\tilde{q}_c)^2}{(1 + \tilde{q}_c^T \tilde{q}_c)^2} \quad (12)$$

C. Relative Kinematics and Dynamics of Satellites

Let the relative translational position and the relative translational velocity of the chaser satellite with respect to the target satellite is given by $\tilde{e}_p = \tilde{p}_c - \mathbf{B}_t^c \tilde{p}_t$ and $\tilde{e}_v = \tilde{v}_c - \mathbf{B}_t^c \tilde{v}_t$, respectively. The relative acceleration of chaser satellite with respect to the target satellite can be described as shown below.

$$\begin{aligned} \dot{\tilde{e}}_v = & \frac{\tilde{F}_c}{M_c} + \frac{\tilde{F}_{j_2,c}}{M_c} + \frac{\tilde{F}_{dc}}{M_c} + (\mathbf{\Omega}(\tilde{e}_\omega) + \mathbf{\Omega}(\tilde{\omega}_t)) \mathbf{B}_t^c \tilde{v}_t \\ & - \mathbf{\Omega}(\tilde{\omega}_c) \tilde{v}_c - \mathbf{B}_t^c \frac{\tilde{F}_{dt}}{M_t} \end{aligned}$$

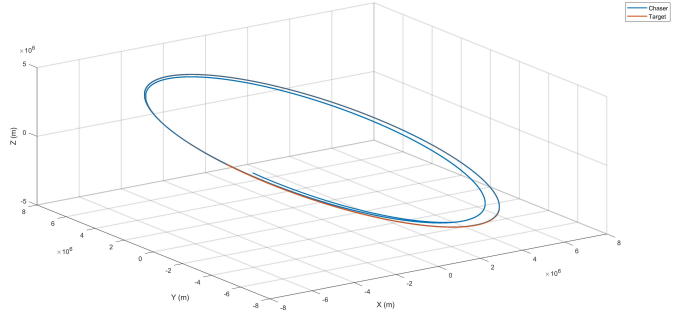


Fig. 2. Plot of 3D trajectory of chaser satellite and target satellite in ICRF Frame during rendezvous maneuver

Relative translational dynamics is obtained by multiplying the above equation with mass of chaser satellite M_c yields

$$\begin{aligned} M_c \dot{\tilde{e}}_v + M_c \mathbf{\Omega}(\tilde{\omega}_c) \tilde{v}_c = & \tilde{F}_c + \tilde{F}_{j_2,c} + \tilde{F}_{dc} - M_c \mathbf{B}_t^c \frac{\tilde{F}_{dt}}{M_t} + \\ & M_c (\mathbf{\Omega}(\tilde{e}_\omega) + \mathbf{\Omega}(\tilde{\omega}_t)) \mathbf{B}_t^c \tilde{v}_t \end{aligned} \quad (13)$$

The relative attitude tracking error of chasersatellite w.r.t target satellite is given by $\tilde{e}_r = \tilde{q}_c - \tilde{q}_t$. The relative angular velocity vector of chaser satellite w.r.t target satellite is expressed as $\tilde{e}_\omega = \tilde{\omega}_c - \mathbf{B}_t^c \tilde{\omega}_t$, where $\mathbf{B}_t^c \in \mathbb{R}^{3 \times 3}$ denotes the rotation matrix from the E_t to E_c and is formulated as $\mathbf{B}_t^c = (\mathbf{B}_c^i)^T \mathbf{B}_t^i$ using (12) and (7). The relative angular acceleration is given by performing time-derivative as shown below.

$$\dot{\tilde{e}}_\omega = \dot{\tilde{\omega}}_c + \tilde{\omega} \times \mathbf{B}_d^c \omega_d - \mathbf{B}_d^c \dot{\tilde{\omega}}_d$$

where subscript $(\cdot)_d$ represents the desired position or orientation to be achieved by the chaser satellite at the end of docking phase. Relative rotational dynamics is obtained by multiplying the above equation by \mathbf{J}_c as shown below.

$$\mathbf{J}_c \dot{\tilde{e}}_\omega = \mathbf{J}_c \dot{\tilde{\omega}}_c + \mathbf{J}_c \tilde{\omega} \times \mathbf{B}_d^c \omega_d - \mathbf{J}_c \mathbf{B}_d^c \dot{\tilde{\omega}}_d \quad (14)$$

III. TRAJECTORY OPTIMIZATION

The optimization problem aims to minimize the chaser satellite's impulse via the objective function:

$$J = \text{minimize} \left(\sum_{i=1}^n \Delta v_i \right)^2$$

subject to nonlinear inequality constraints:

(a) **Spherical keep-out zone**: $\|\tilde{e}_p\| \geq R_{min}$
Maintains a minimum distance R_{min} from the target to prevent collisions as shown in Fig. 1(a).

(b) **Approach conic corridor**: $\|\tilde{e}_p\| \cos(\alpha_{cone}) \leq \hat{1}_t \tilde{e}_p$
Confines the chaser within a cone (half-angle α_{cone}) aligned with the target's docking axis $\hat{1}_t$ during terminal approach as illustrated in Fig. 1(a).

(c) **Field of view constraint**: $\|\tilde{e}_{FOV}\| \cos(\alpha_{FOV}) \leq \hat{1}_c \tilde{e}_{FOV}$

Ensures continuous target visibility within the chaser's sensor cone half-angle α_{FOV} along its docking axis $\hat{\mathbf{l}}_c$ as depicted in Fig. 1(b), where $\tilde{\mathbf{e}}_{FOV}$ is the relative position vector of target satellite w.r.t chaser satellite.

(e) **Velocity Constraint:** This constraint enforce a constant velocity of 0.3 m/s during mid-range proximity maneuver from 1 km to 10 m and reduces it to 0.03 m/s for final soft docking.

$$\tilde{v} = \begin{cases} 0.3\text{ m/s} & , \text{if } 10\text{ m} < \|\tilde{\mathbf{e}}_p\| \leq 1000\text{ m} \\ 0.03\text{ m/s} & , \text{if } \|\tilde{\mathbf{e}}_p\| \leq 10\text{ m} \end{cases}$$

(e) **Impulse Constraint:** $-300\sqrt{3} < \|\Delta v\| < 300\sqrt{3}$

IV. DESIGN OF CROSS-FEEDBACK SLIDING MODE CONTROLLER

In this section, we have implemented a cross-feedback sliding mode controller (CxSMC) to track the trajectory for the chaser satellite in the three-dimensional configuration space SE(3). Stability of the controller is established using a Lyapunov framework.

Lemma 1: For a nonlinear system expressed as $\dot{\tilde{y}} = f(\tilde{y})$, $\tilde{y}(0) = \tilde{y}_0$, $\tilde{y} \in \mathbb{R}^n$, if there exist a continuously differentiable Lyapunov function $V(x)$ in the neighborhood $N \subset \mathbb{R}^n$ of origin, which satisfies $\dot{V}(\tilde{y}) \leq -kV(\tilde{y})$ where $k > 0$. Then the origin of the system is asymptotically stable and the settling time $T(y)$ is dependent on initial states as shown below.

$$T(y) \leq T_{max} = \frac{\ln(V)}{k}$$

A. Cross-Feedback Linear Sliding Surface

Instead of designing independent sliding surfaces for translational and rotational motion, the proposed cross-feedback sliding surface of translational motion consists of translational error and cross-feedback terms of rotational error and vice versa. The translational sliding surface denoted by \tilde{s}_p (15) and the rotational sliding surface denoted by \tilde{s}_r (16) is defined based on relative position $\tilde{\mathbf{e}}_p$ and orientation error $\tilde{\mathbf{e}}_r$ as shown below.

$$\tilde{s}_p = \dot{\tilde{\mathbf{e}}}_p + \lambda_p \tilde{\mathbf{e}}_p + \mu_p \tilde{\mathbf{e}}_r \quad (15)$$

$$\tilde{s}_r = \dot{\tilde{\mathbf{e}}}_r + \lambda_r \tilde{\mathbf{e}}_r + \mu_r \tilde{\mathbf{e}}_p \quad (16)$$

where $\lambda_p, \lambda_r > 0$ and $\mu_p, \mu_r > 0$ are cross-feedback gains. An exponential reaching law for both translational and rotational motion is defined to ensure that the system error states reaches the sliding surface as, $\dot{\tilde{s}}_p = -k_p \tilde{s}_p$ and $\dot{\tilde{s}}_r = -k_r \tilde{s}_r$

Theorem 1 (Stability of Reaching Phase) If the cross-feedback sliding surface for translational and rotational motion is defined as shown in (15) and (16), respectively for the relative translational and rotational dynamics described in (13) and (14), the relative position and velocity of the chaser satellite with respect to the target satellite will converge to the sliding

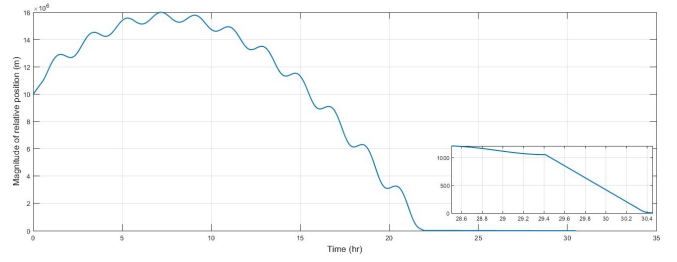


Fig. 3. Relative position of chaser satellite with respect to target satellite

surface. The control force and torque acting on the chaser satellite is given as

$$\begin{aligned} \tilde{\mathbf{F}}_c = & -\tilde{\mathbf{F}}_{j_2,c} - \tilde{\mathbf{F}}_{dc} - M_c (\boldsymbol{\Omega}(\tilde{\mathbf{e}}_\omega) + \boldsymbol{\Omega}(\tilde{\omega}_t)) B_t^c \tilde{v}_t \\ & + M_c \boldsymbol{\Omega}(\tilde{\omega}_c) \tilde{v}_c + B_t^c \left(\frac{M_c}{M_t} \right) \tilde{\mathbf{F}}_{dt} - \lambda_p M_c \dot{\tilde{\mathbf{e}}}_p \\ & - \mu_p M_c \dot{\tilde{\mathbf{e}}}_r - k_p \tilde{s}_p \end{aligned} \quad (17)$$

$$\begin{aligned} \tilde{\mathbf{T}}_c = & -\tilde{\mathbf{T}}_{dc} - \tilde{\mathbf{T}}_{gc} + \boldsymbol{\Omega}(\tilde{\omega}_c) \mathbf{J}_c \tilde{\omega}_c - \mathbf{J}_c \tilde{\mathbf{e}}_\omega \times \mathbf{B}_d^c \dot{\tilde{\omega}}_d \\ & + \mathbf{J}_c \mathbf{B}_d^c \dot{\tilde{\omega}}_d - \lambda_r \mathbf{J}_c \dot{\tilde{\mathbf{e}}}_r - \mu_r \mathbf{J}_c \dot{\tilde{\mathbf{e}}}_p - k_r \tilde{s}_r \end{aligned} \quad (18)$$

Proof: Consider a continuous differentiable Lyapunov function as

$$V_1 = \frac{1}{2} \tilde{s}_p^T \mathbf{M}_c \tilde{s}_p + \frac{1}{2} \tilde{s}_r^T \mathbf{J}_c \tilde{s}_r$$

The time derivative of Lyapunov function can be written using (17) and (18)

$$\begin{aligned} \dot{V}_1 = & \tilde{s}_p^T M_c \dot{\tilde{s}}_p + \tilde{s}_r^T \mathbf{J}_c \dot{\tilde{s}}_r \\ = & -k_p \tilde{s}_p^T M_c \tilde{s}_p - k_r \tilde{s}_r^T \mathbf{J}_c \tilde{s}_r \\ \leq & -\lambda_1 (\tilde{s}_p^T M_c \tilde{s}_p) - \lambda_1 (\tilde{s}_r^T \mathbf{J}_c \tilde{s}_r) \end{aligned}$$

where $\lambda_1 = \min(k_p, k_r)$. The Lyapunov derivative can be rewritten as

$$\begin{aligned} \dot{V}_1 \leq & -\lambda_1 (\tilde{s}_p^T M_c \tilde{s}_p + \tilde{s}_r^T \mathbf{J}_c \tilde{s}_r) \\ \leq & -\lambda_1 (2V_1) \\ \leq & -\lambda_2 V_1 \end{aligned}$$

where $\lambda_2 = 2\lambda_1$ and $\lambda_2 > 0$. It can be inferred from the lyapunov derivative $\dot{V}_1 \leq 0$ that the system is asymptotically stable according to Lemma 1. Consequently, the error states converges to the desired sliding surface of translational and rotational motion $\tilde{s}_p = 0$ and $\tilde{s}_r = 0$ in finite time.

Theorem 2 (Stability of Sliding Phase) If the cross-feedback sliding surface for translational and rotational motion is defined as shown in (15) and (16), respectively for the relative translational and rotational dynamics described in (13) and (14), the relative position and velocity of the chaser satellite with respect to the target satellite will converge to equilibrium along the sliding surface in finite time.

$$T_s(x) \leq \frac{\ln(V_2)}{\lambda_4}$$

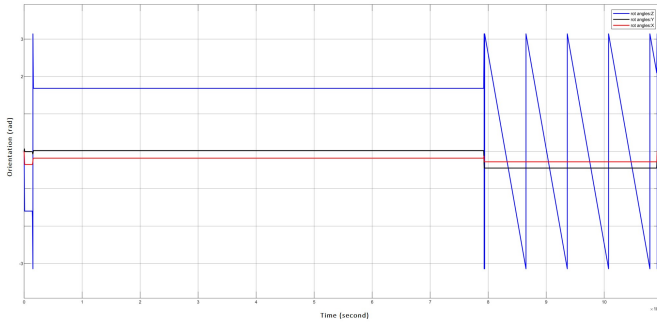


Fig. 4. Relative orientation performed by chaser satellite to dock with the target satellite

Proof: Consider a continuous differentiable Lyapunov function as

$$V_2 = \frac{1}{2} \tilde{e}_p^T \tilde{e}_p + \frac{1}{2} \tilde{e}_r^T \tilde{e}_r$$

The time derivative of Lyapunov function is

$$\dot{V}_2 = \tilde{e}_p^T \dot{\tilde{e}}_p + \tilde{e}_r^T \dot{\tilde{e}}_r$$

when the error states evolve on the sliding surface i.e. $\tilde{s}_p = 0$ and $\tilde{s}_r = 0$, then $\dot{\tilde{e}}_p$ and $\dot{\tilde{e}}_r$ are given by $\dot{\tilde{e}}_p = -\lambda_p \tilde{e}_p - \mu_p \tilde{e}_r$ and $\dot{\tilde{e}}_r = -\lambda_r \tilde{e}_r - \mu_r \tilde{e}_p$. The Lyapunov derivative can be rewritten as

$$\begin{aligned} \dot{V}_2 &= -\tilde{e}_p^T (\lambda_p \tilde{e}_p + \mu_p \tilde{e}_r) - \tilde{e}_r^T (\lambda_r \tilde{e}_r + \mu_r \tilde{e}_p) \\ &= -\lambda_p \tilde{e}_p^T \tilde{e}_p - \lambda_r \tilde{e}_r^T \tilde{e}_r - (\mu_p + \mu_r) \tilde{e}_p^T \tilde{e}_r \\ &\leq -\lambda_p \tilde{e}_p^T \tilde{e}_p - \lambda_r \tilde{e}_r^T \tilde{e}_r \\ &\leq -\lambda_3 (\tilde{e}_p^T \tilde{e}_p + \tilde{e}_r^T \tilde{e}_r) \\ &\leq -\lambda_3 (2V_2) \\ \dot{V}_2 &\leq -\lambda_4 V_2 \end{aligned}$$

where $\lambda_3 = \min(\lambda_p, \lambda_r)$, $\lambda_4 = 2\lambda_3$ and $\lambda_4 > 0$. It can be inferred from the Lyapunov derivative $\dot{V}_2 \leq 0$ that the system is asymptotically stable by Lemma 1. Consequently, the error states converge to the equilibrium point along the desired sliding surface of translational and rotational motion $\tilde{s}_p = 0$ and $\tilde{s}_r = 0$ in finite time.

V. RESULTS AND DISCUSSION

The mass of both the satellite are considered to be 1000 kg. And the inertia matrix of both satellites are taken as $\mathbf{J}_t = \text{diag}(500, 2500, 2500) \text{ kg-m}^2$. The initial classical orbital elements of the chaser and target satellite is given in Table I. The three-dimensional trajectory of chaser and target satellite during rendezvous and docking maneuver is shown in Fig. 2.

The initial relative position of the chaser satellite w.r.t the target satellite is specified as 10,000 km. This marks the starting point of the rendezvous and docking mission, where the primary objective is to bring the chaser satellite into close proximity with the target satellite in a controlled and precise manner. The rendezvous condition is achieved when the radial

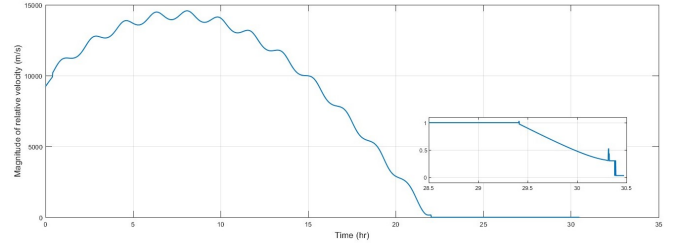


Fig. 5. Relative velocity of chaser satellite with respect to the target satellite

distance between the chaser and target satellite reduces to 1 km which occurs at a mission duration of 29 hr 24 min as illustrated in Fig. 3. At this point the chaser satellite transitions into the docking phase, which is executed in two distinct phases to ensure safety and precision while avoiding any potential impact at the conclusion of the maneuver.

In the first phase of the docking process, the relative velocity between the chaser and target satellite is maintained at a constant value of 0.3 m/s until the relative position decreases to 10 m. This ensures that the chaser satellite approaches the target satellite steadily and predictably. Once the relative position reduces to 10 m, the second phase commences, during which the relative velocity is further reduced to 0.03 m/s. This reduction in velocity is critical for achieving a soft and precise docking, minimizing any risk of collision or damage to either satellite. The relative velocity during entire docking process is depicted in Fig. 5, highlighting the controlled deceleration during both the phases. Successful docking is confirmed after a total mission duration of 30 hr 28 min 29 sec, with the final separation distance between the centers of mass (c.m.) of the chaser and target satellites being 1 m. The optimization

TABLE I
INITIAL ORBITAL ELEMENTS OF THE CHASER AND TARGET SATELLITE

Parameters	Chaser	Target
Semi major axis (km)	7500	8000
Eccentricity	0.001	0.0005
Inclination ($^\circ$ deg)	30.1	30
RAAN ($^\circ$ deg)	60.1	60
Argument of Periapsis (deg)	120	120
True anomaly ($^\circ$ deg)	30	310

of mission results based on on constraints outlined in Section III results in a total impulse ΔV of 237.0428 m/s, which represents the cumulative velocity change required for the chaser satellite to complete its maneuver. The maximum burn duration for any single thruster firing is recorded to be 4.9 ms, reflecting the high precision and efficiency of the propulsion system. In addition to translational motion, the mission also involves careful management of the chaser satellite's orientation. Initially, the relative orientation of the chaser satellite with respect to the target is (0, 0, 0) radians, and the relative angular velocity is (0, 0, 0) radians per second as shown in Fig. 4 and Fig. 6, respectively. By the end of the docking phase, the chaser satellite must achieve a relative orientation of $(\pi, \pi, 0)$ radians with respect to the target satellite. To accomplish this,

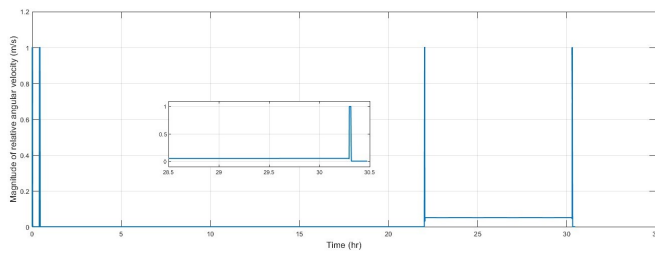


Fig. 6. Relative angular velocity of chaser satellite with respect to the target satellite

the chaser satellite performs a rotational maneuver involving Euler angles $(\phi, \theta, \psi) = (0, 0, -\pi)$ radians, as observed at the end of simulation in Fig. 4.

Notably, the rendezvous condition is met within 22 hrs, during which the relative velocity is successfully reduced to 1km/s, as demonstrated in Fig. 3 and Fig. 5. This highlights the effectiveness of the trajectory planning and control algorithms employed during the mission. The combination of precise velocity control, optimized thrust maneuvers, and accurate rotational adjustments ensures that the chaser satellite achieves its objectives safely and efficiently, culminating in a successful docking operation.

VI. CONCLUSION

The proposed work introduces a cross-feedback sliding mode controller for satellite rendezvous and docking (RvD). By integrating cross-feedback mechanisms, the controller interdependently regulates translational and rotational motions of the chaser satellite, utilizing rotational state data to inform translational control laws and vice versa. This approach decouples relative motion dynamics between the chaser and target satellites for simplified design while explicitly accounting for their inherent coupling.

REFERENCES

- [1] Y. Xie, C. Chen, T. Liu, and M. Wang, "Guidance, Navigation, and Control for Spacecraft Rendezvous and Docking: Theory and Methods," *Guidance, Navigation, and Control for Spacecraft Rendezvous and Docking: Theory and Methods*, 2021, doi: 10.1007/978-981-15-6990-6.
- [2] S. Di Cairano, H. Park, and I. Kolmanovsky, "Model Predictive Control approach for guidance of spacecraft rendezvous and proximity maneuvering," *International Journal of Robust and Nonlinear Control*, vol. 22, no. 12, pp. 1398–1427, Aug. 2012, doi: 10.1002/RNC.2827.
- [3] Q. Hu, W. Chen, and L. Guo, "Fixed-Time Maneuver Control of Spacecraft Autonomous Rendezvous with a Free-Tumbling Target," *IEEE Trans Aerosp Electron Syst*, vol. 55, no. 2, pp. 562–577, Apr. 2019, doi: 10.1109/TAES.2018.2852439.
- [4] K. Xia and W. Huo, "Adaptive control for spacecraft rendezvous subject to actuator faults and saturations," *ISA Trans*, vol. 80, pp. 176–186, Sep. 2018, doi: 10.1016/J.ISATRA.2018.07.030.
- [5] F. Stesina, "Tracking Model Predictive Control for Docking Maneuvers of a CubeSat with a Big Spacecraft," *Aerospace*, vol. 8, no. 8, Aug. 2021, doi: 10.3390/AEROSPACE8080197.
- [6] A. Kosari, H. Jahanshahi, and S. A. Razavi, "An optimal fuzzy PID control approach for docking maneuver of two spacecraft: Orientational motion," *Engineering Science and Technology, an International Journal*, vol. 20, no. 1, pp. 293–309, Feb. 2017, doi: 10.1016/J.JESTCH.2016.07.018.

- [7] A. J. Cavaciuti, J. H. Heying, and J. Davis, "In-space servicing, assembly, and manufacturing for the new space economy," Center for space policy and strategy.
- [8] Q. Li, J. Yuan, B. Zhang, and C. Gao, "Model predictive control for autonomous rendezvous and docking with a tumbling target," *Aerosp Sci Technol*, vol. 69, pp. 700–711, Oct. 2017, doi: 10.1016/J.AST.2017.07.022.
- [9] G. Arantes and L. S. Martins-Filho, "Guidance and Control of Position and Attitude for Rendezvous and Dock/Berthing with a Noncooperative/Target Spacecraft," *Math Probl Eng*, vol. 2014, no. 1, p. 508516, Jan. 2014, doi: 10.1155/2014/508516.
- [10] N. D- and by D. Robert Langley, "Apollo experience report: The docking system," 1972.
- [11] D. Malladi, S.; Cairano, A. Weiss, "Nonlinear Model Predictive Control of Coupled Rotational-Translational Spacecraft Relative Motion," 2019, doi: 10.23919/ACC.2019.8814345.
- [12] R. K. Sahoo and M. Sinha, "Coupled Rendezvous and Docking Maneuver Control of Spacecraft using Fast Fixed-Time Sliding Mode Controller," *IAF Astrodynamics Symposium*, pp. 1028–1042, 2024, doi: 10.52202/078368-0087.
- [13] K. Gong, Y. Liao, and Y. Wang, "Adaptive Fixed-Time Terminal Sliding Mode Control on SE(3) for Coupled Spacecraft Tracking Maneuver," *International Journal of Aerospace Engineering*, vol. 2020, 2020, doi: 10.1155/2020/3085495.
- [14] R. Kumar Sahoo and M. Sinha, "Coupled Rendezvous and Docking Maneuver control of satellite using Reinforcement learning-based Adaptive Fixed-Time Sliding Mode Controller," Feb. 2025, doi: 10.48550/arXiv.2502.09517.
- [15] D. Lee, "Spacecraft Coupled Tracking Maneuver Using Sliding Mode Control with Input Saturation," *J Aerosp Eng*, vol. 28, no. 5, Sep. 2015, doi: 10.1061/(asce)as.1943-5525.000047.
- [16] A. M. Gontier *et al.*, "Establishment of the ICRF," *Advances in Space Research*, vol. 30, no. 2, pp. 185–193, Jul. 2002, doi: 10.1016/S0273-1177(02)00283-1.